



ELSEVIER

Chemical Physics 190 (1995) 393–405

Chemical
Physics

The intramolecular dynamics of allene in the region around 6000 cm^{-1} via eigenstate resolved IR spectroscopy

J.H. Timmermans, K.K. Lehmann, G. Scoles

Princeton University, Department of Chemistry, Princeton, NJ 08544, USA

Received 31 May 1994; in final form 30 September 1994

Abstract

We have recorded and analyzed the molecular beam spectra of allene in the regions of the $\nu_1 + \nu_5$ and $2\nu_8$ bands around 5947.5 and 6135.5 cm^{-1} , respectively. The $\nu_1 + \nu_5$ band only shows minor perturbations and we suspect the presence of a doorway state that causes parallel Coriolis coupling to the bath states. Perpendicular Coriolis interactions do not seem to play an important role since the size of the matrix elements does not increase systematically with J' . The spectrum in the region of the $2\nu_8$ band is more complicated; a total of six sub-bands has been identified with $K=0-2$. Based on the lack of any systematic dependence on J' and an inverse dependence of the coupling on K , we expect that neither parallel nor perpendicular Coriolis coupling is present in this band. The effective lifetime for both bands is calculated to be about 200 ps, which is very similar to the lifetimes of an acetylenic C–H stretch overtone.

1. Introduction

One of the central goals of chemical physics is to understand vibrational energy flow in molecules because of its importance in many fundamental chemical and physical processes and because of its practical applications to the chemistry of vibrationally excited species. Over the past decade several research groups have studied intramolecular vibrational energy redistribution (IVR) in medium to large poly-atomic molecules, using high resolution IR spectroscopy in supersonic jets and beams (for a review of the field of IVR see Ref. [1]). It has been found that many of the spectra of these molecules are perturbed through very weak near resonant couplings to a background of vibrational states. For example, Perry's group reported that in 1-butyne at low temperature, the $K'_a = 1$ transitions were not perturbed, but the $K'_a = 0$ levels were split into multiplets [2]. They concluded that the $K'_a = 0$ levels

are mixed with the bath of the background vibrations by anharmonic matrix elements of the order of 0.01 cm^{-1} .

One of the benchmark molecules in the field of IVR is propyne. McIlroy and Nesbitt have investigated the ν_1 band, i.e. the acetylenic C–H stretch fundamental [3]. This band was recently re-investigated by Kerstel et al. [4] using a weak expansion which results in a warmer spectrum (30–50 K) that includes up to $K=6$ states. They found that each K sub-band can be fit to within a few MHz, but that the positions of the sub-bands point to long range perturbations by at least two background states. In a separate publication, McIlroy and Nesbitt and our Princeton group investigated the $2\nu_1$ band [5]. In this case it was found that the coupling between the bright state and the dark states is mediated by one or more doorway state(s) that is (are) anharmonically coupled to the bright state and is (are) z -axis Coriolis coupled to the bath states. A state that

Table 1
Normal modes of allene

Mode	Frequency	Symmetry	Motion
ν_1	3014.4	A ₁	C–H stretch
ν_2	1443.3	A ₁	C–H bend/scissor
ν_3	1072.1	A ₁	C=C=C stretch
ν_4	848.59	B ₁	CH ₂ torsion
ν_5	3006.72	B ₂	C–H stretch
ν_6	1959.38	B ₂	C=C=C stretch
ν_7	1395	B ₂	C–H bend/scissor
ν_8	3085.53	E	C–H anti symmetric stretch
ν_9	999.0	E	CH ₂ rock in individual planes
ν_{10}	840.9	E	CH ₂ wagging orthogonal to plane
ν_{11}	352.73	E	C=C=C bend

appears to be acting as such a doorway state has been detected by Go and Perry [6] using IR–IR double resonance techniques. Using similar bolometer detected double resonance, our group has recently reported the analysis of the $3\nu_1$ band of propyne as well [7].

One of the aims of these type of studies is to correlate the vibrational energy relaxation rates of a molecule to its structure. Bethardy et al. [8] have proposed to correlate the acceleration of IVR with the proximity of the initially excited vibration to bonds that give rise to flexibility and conformational change (centers of flexibility). However, there is a high correlation between the type of bond and the distance to the centers of flexibility. For example, most of the research to date on molecules without centers of flexibility has been concentrated on terminal acetylenes. Therefore it would be desirable to study other rigid molecules containing different kind of chromophores.

In this context allene is a very interesting molecule since it is quite rigid and therefore exhibits no internal rotation (the barrier for racemization is about 2.04 eV [9]). Furthermore, allene is an isomer of propyne. They have very similar calculated densities of states at 6000 cm⁻¹: 35.9 states per cm⁻¹ in propyne versus 27.9 states per cm⁻¹ in allene (direct anharmonic count over a 100 cm⁻¹ interval).

Allene has been studied extensively, both theoretically and experimentally [10–25]. It has normal modes of the A₁, B₁, B₂ or E symmetry. Only the B₂ and E modes show infrared activity. Table 1 lists all the normal modes with their frequency, symmetry and the motion involved. The fundamental ν_5 and the ν_8 bands and the A₁A₂–E and B₁B₂–E components of the

$\nu_8 + \nu_{11} - \nu_{11}$ hot band were investigated by Maki et al. [22]. They observed a splitting of the Q branches in the fundamental caused by a large perturbation with a coupling matrix element of the order of 0.7 cm⁻¹. Many other weaker perturbations in the fundamental bands induced a shift of the levels of about 0.02 cm⁻¹. The least perturbed lines have been used to fit intensity parameters for both bands. The ν_{11} band has been investigated by Pliva and Kauppinen [21]. These authors combined their data with published Raman data to obtain improved estimates for the rotational constant A_0 and the centrifugal constant D_K^0 . More recently, Hegelund et al. [25] determined these ground state rotational and centrifugal constants from a simultaneous analysis of the ground state combination differences of five bands: the ν_9 , ν_{10} , ν_{11} and $\nu_{11}^{\pm 1} + \nu_9^{\pm 1}$, $\nu_{11}^{\pm 1} + \nu_9^{\pm 1} - \nu_{11}^{\pm 1}$ bands.

In this paper we report on the rotationally resolved $\nu_1 + \nu_5$ and $2\nu_8$ spectra of allene in the region around 5947.5 cm⁻¹ and around 6135.5 cm⁻¹, respectively. We observe one strong band near 5947.5 cm⁻¹, which is weakly perturbed by z-axis Coriolis coupling with matrix elements between 0.001 and 0.02 cm⁻¹. In the higher energy region six sub bands have been assigned (three $K=0$, two $K=1$ and one $K=2$). Each of these sub bands shows weak perturbations by other levels.

2. Experimental

The spectrometer used in these experiments is based on the optothermal detection of the energy deposited by a cw tunable infrared laser in a collimated supersonic molecular beam, which has been described extensively in the literature [27,28]. Our spectrometer is discussed in detail in reference [29]. A brief description is given below.

A 1% mixture of allene (Aldrich) in helium (Matheson) is expanded through a 50 μm diameter pinhole at room temperature at a stagnation pressure of about 4 atm. A 500 μm skimmer, placed 12 mm downstream from the nozzle, defines the collimated molecular beam. Approximately 44 cm downstream from the skimmer, the beam impinges upon a liquid helium cooled bolometer. The molecules in the beam interact with laser radiation in a multipass cell that is placed between the skimmer and the bolometer. The multipass consists of two plano parallel, gold coated mirrors

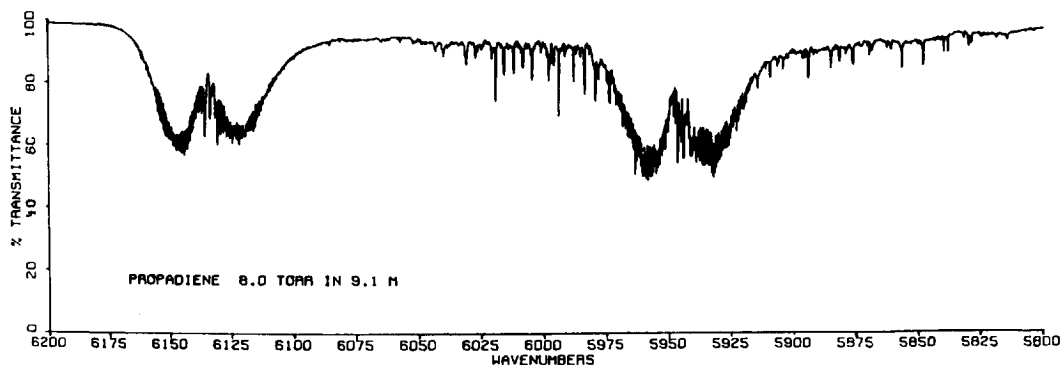


Fig. 1. FT-IR spectrum of allene in the 6000 cm^{-1} region, recorded by Mills and Mompean. As it can be seen, in the region of the $\nu_1 + \nu_5$ band, there are several strong perpendicular Q branches. Mills and Mompean assigned these to the $\nu_1 + \nu_8$ band. The $\nu_5 + \nu_8$ band, predicted to be centered around 6096 cm^{-1} is obscured by the much stronger $2\nu_8$ band at 6135.5 cm^{-1} . (Reproduced with the permission of I.M. Mills.)

which are separated by precision quartz spacers. The length of the interaction region is about 10 cm. Laser radiation is supplied by a Burleigh model 220 color center laser. This laser is pumped by 4 W of $1.064\text{ }\mu\text{m}$ and 6 mW of 532 nm radiation from Spectra Physics 3460 modelocked Nd:YAG laser. The color center laser is tunable from 1.5 to $1.7\text{ }\mu\text{m}$ and delivers a maximum of 200 mW at $1.6\text{ }\mu\text{m}$. An 80286 personal computer controls the scanning of the laser, and records the data. The wavelength is measured with a traveling mirror wavemeter, with a resolution of 0.001 cm^{-1} . The wavemeter is calibrated against the spectrum of acetylene, observed in a static cell. We estimate that the absolute frequency is accurate to $\pm 0.005\text{ cm}^{-1}$.

The spectra reported below have an instrument limited linewidth of 15 MHz full width at half maximum. This linewidth results from a combination of several factors, including Doppler broadening due to the slight angle ($\sim 2^\circ$) the laser beam makes with the normal to the molecular beam and laser frequency jitter (~ 8 MHz).

3. Results and discussion

Both the $\nu_1 + \nu_5$ and the $2\nu_8$ bands in allene were recorded and analyzed in 1969 by Nguyen van Than [29]. More recently Mills and Mompean used the same bands to study mode localization effects [30]. They derived general relations between the anharmonic x_{rs} constants and the Darling–Dennison constants K_{rrss} for stretching vibrations which allow local-mode effects to

be generated by adding the appropriate anharmonic and Darling–Dennison constants to the familiar normal mode model of molecular vibrations. Fig. 1 shows an FTIR spectrum of allene from 5800 to 6200 cm^{-1} . Both bands are readily observed and exhibit the familiar parallel band contours. As can be seen from the spectrum, there are many strong perpendicular Q branches in the region around 5980 cm^{-1} . Mills and Mompean assigned these Q branches to the $\nu_1 + \nu_8$ vibrational band. They also predicted that the $\nu_5 + \nu_8$ band be centered around 6096 cm^{-1} (with an uncertainty of about 20 cm^{-1}). However, as can be seen from the FTIR spectrum, the observation of this band is obscured by the much stronger $2\nu_8$ parallel band. We have calculated the character of both parallel bands in the normal mode and local mode pictures using the Hamiltonian given by Mills and Mompean. For the normal mode picture we find:

$$\begin{aligned} &(\text{upper state})_{5947.5\text{ cm}^{-1}\text{ band}} \\ &= 0.94|\nu_1 + \nu_5\rangle + 0.34|2\nu_8^{\pm 2}, B_2\rangle, \end{aligned}$$

$$\begin{aligned} &(\text{upper state})_{6135.5\text{ cm}^{-1}\text{ band}} \\ &= -0.34|\nu_1 + \nu_5\rangle + 0.94|2\nu_8^{\pm 2}, B_2\rangle. \end{aligned}$$

In this case the two basis states are coupled by a matrix elements of -56 cm^{-1} . In the local mode picture we can generate two states of B_2 symmetry:

$$\begin{aligned} |2, 0, 0, 0; B_2\rangle &= \frac{1}{2}(|2, 0, 0, 0\rangle + |0, 2, 0, 0\rangle \\ &\quad - |0, 0, 2, 0\rangle - |0, 0, 0, 2\rangle), \end{aligned}$$

$$|1, 1, 0, 0; B_2\rangle = \frac{1}{\sqrt{2}}(|1, 1, 0, 0\rangle - |0, 0, 1, 1\rangle).$$

The four labels indicate the number of quanta in each of the four C–H bonds, with bonds 1 and 2 sharing the same carbon atom. Using this basis, we can calculate the character of the two upper states for the two bands:

(upper state)_{5947.5 cm⁻¹ band}

$$= 0.88|2, 0, 0, 0; B_2\rangle + 0.48|1, 1, 0, 0; B_2\rangle,$$

(upper state)_{6135.5 cm⁻¹ band}

$$= -0.48|2, 0, 0, 0; B_2\rangle + 0.88|1, 1, 0, 0; B_2\rangle.$$

From these calculations we can conclude that the normal mode is more accurate than the local mode picture in describing the character of both bands. Therefore we can label them predominantly by their normal mode assignment. Below we discuss each of the two bands separately.

3.1. The $\nu_1 + \nu_5$ band

The $\nu_1 + \nu_5$ band is a combination of two C–H stretching motions. It is of B_2 symmetry, and therefore the usual parallel polarization selection rules $\Delta J = 0, \pm 1$ and $\Delta K = 0$ apply. The spectrum, shown in Fig. 2, was recorded from 5943 to 5951 cm⁻¹ from the P(7) to the R(5) transitions, both included. Table 2 lists the experimental frequencies and relative intensities of the

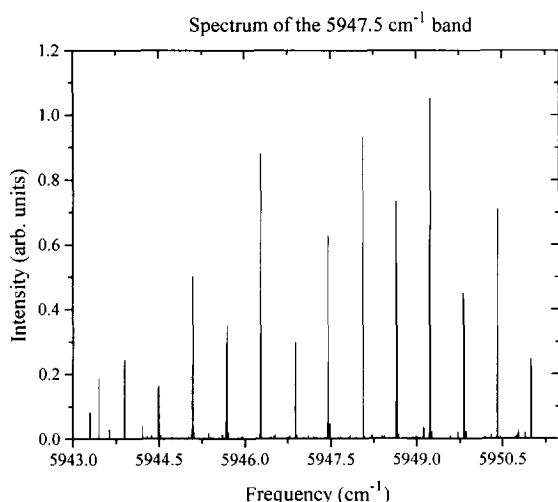


Fig. 2. Spectrum of the $\nu_1 + \nu_5$ band in the 5947.5 cm⁻¹ region. Note the small Q branch just to the right of the 5950.5 cm⁻¹ marker. This is very likely a $K=1$ Q-branch belonging to the $\nu_1 + \nu_8$ band. Also, note the intensity spin alternation for J' .

observed transitions. Relative intensities of nearby lines are estimated to be precise to approximately 10% based upon previous experience. The accuracy of the absolute frequency is limited by the resolution of our wave meter and the acetylene calibration standard which is estimated at ± 0.005 cm⁻¹. The transitions were assigned using the ground-state combination differences method using the ground state constants from Ref. [25]. We were able to assign about 75% of the observed transitions, including all the strong lines. Some of the unassigned lines are most likely transitions of another band, probably the perpendicular $\nu_1 + \nu_8$ band. Note the small Q branch observed at 5950.75 cm⁻¹. We suspect that this is a $K=1$ Q branch, also belonging to the $\nu_1 + \nu_8$ band. The ground-state combination differences of all the assigned lines were well within the experimental error of about 15 Mhz.

The spin statistics for allene have been worked out by Maki et al.; the even K values in the ground state have a spin statistical weight of 10, while the odd K values have a weight of 6. For $K=0$ levels, those with an even J value have a spin weight of 7 and odd J levels have a weight of 3. This spin alternation of the $K=0$ lines is evident in Fig. 2. Since the temperature of our beam is approximately 5 K we observe only $K=0, 1$ and 2 states. Intensity fluctuations within each J clump often obscure the spin statistics for the individual K states in this spectrum.

We carried out a linear least square fit of assigned transitions to the transition frequencies expected for a parallel band of a symmetric top molecule. For P and R branch transitions this frequency can be written as

$$\begin{aligned} \nu_{m,K}^{P,R} = & \nu_0 + (B' + B'')m + (B' - B'' - D'_j + D''_j)m^2 \\ & - 2(D'_j + D''_j)m^3 - (D'_j - D''_j)m^4 \\ & + \{[(A' - B') - (A'' - B'')] - [D'_{JK} + D''_{JK}]m \\ & - [D'_{JK} + D''_{JK}]m^2\}K^2, \end{aligned} \quad (1)$$

in which $m = J + 1$ for the R branch and $m = -J$ for the P branch. Ground-state constants were constrained to those of Ref. [25]. Table 3 lists the results of the fit for each of the individual sub bands. Adding the ΔD_j constant increased the value of σ^2 . Therefore the upper state values for D_j were kept at the ground-state constant values from reference [25]. The values for D''_{JK} and D'_{JK} were also fixed at their ground-state values, since only one sub-band was fit at a time. When the

Table 2

Line positions and relative intensities for the transitions observed in the 5947.5 cm⁻¹ region

	Frequency (cm ⁻¹)	Relative intensity		Frequency (cm ⁻¹)	Relative intensity
^o P ₁ (7)	5943.2862	0.0807	^o Q ₂ (4)	5947.4465	0.0538
^o P ₂ (7)	5943.2906	0.0079	^o Q ₁ (3)	5947.4500	0.0888
^o P ₂ (7)	5943.2919	0.009	^o Q ₁ (2)	5947.4535	0.2354
^o P ₂ (7)	5943.2941	0.0078	^o Q ₁ (1)	5947.4549	0.6276
^o P ₀ (7)	5943.3001	0.0793	^r Q ₁ (1)	5947.4842	0.0464
^o P ₂ (6)	5943.8806	0.0038	^o R ₀ (0)	5948.0616	0.9327
^o P ₁ (6)	5943.8847	0.1155	^o R ₀ (0)	5948.2150	0.0108
^o P ₂ (6)	5943.8905	0.0126	^o R ₁ (1)	5948.6317	0.1141
^o P ₂ (6)	5943.8915	0.0189	^o R ₁ (1)	5948.6386	0.7332
^o P ₀ (6)	5943.8990	0.2438	^o R ₀ (1)	5948.6522	0.5411
^o P ₁ (5)	5944.4815	0.1582	^o R ₁ (2)	5949.2088	0.018
^o P ₂ (5)	5944.4840	0.0384	^o R ₂ (2)	5949.2234	0.0434
^o P ₁ (5)	5944.4951	0.0176	^o R ₁ (2)	5949.2278	0.6593
^o P ₀ (5)	5944.4968	0.1622	^o R ₁ (2)	5949.2342	0.0232
^o P ₂ (5)	5944.5259	0.0113	^o R ₀ (2)	5949.2414	1.0519
^o P ₁ (4)	5945.0612	0.0137	^o R ₁ (2)	5949.2619	0.0077
^o P ₂ (4)	5945.0759	0.029	^o R ₂ (2)	5949.2629	0.0213
^o P ₁ (4)	5945.0800	0.2264	^o R ₁ (3)	5949.8142	0.4487
^o P ₁ (4)	5945.0867	0.0066	^o R ₂ (3)	5949.8164	0.0578
^o P ₀ (4)	5945.0935	0.5001	^o R ₁ (3)	5949.8278	0.0418
^o P ₁ (4)	5945.1141	0.0035	^o R ₀ (3)	5949.8297	0.4299
^o P ₂ (4)	5945.1154	0.0197	^o R ₁ (3)	5949.8303	0.0186
^o P ₂ (3)	5945.6675	0.0171	^o R ₂ (3)	5949.8584	0.0226
^o P ₁ (3)	5945.6690	0.0544	^o R ₂ (4)	5950.3978	0.0076
^o P ₁ (3)	5945.6757	0.2966	^o R ₁ (4)	5950.4023	0.3449
^o P ₀ (3)	5945.6892	0.3502	^o R ₂ (4)	5950.4077	0.019
^o P ₂ (3)	5945.7067	0.0199	^o R ₂ (4)	5950.4087	0.0353
^o P ₂ (3)	5945.7080	0.0058	^o R ₀ (4)	5950.4168	0.7086
^o P ₁ (2)	5946.2529	0.0145	^r Q(1)	5950.7143	0.003
^o P ₁ (2)	5946.2699	0.3251	^r Q(1)	5950.7159	0.0042
^o P ₀ (2)	5946.2840	0.8797	^r Q(1)	5950.7314	0.0053
^o P ₁ (2)	5946.2866	0.0189	^r Q(1)	5950.7450	0.0084
^o P ₀ (1)	5946.8776	0.2975	^r Q(1)	5950.7568	0.0103
^o P ₀ (1)	5946.8976	0.012	^r Q(1)	5950.7663	0.0152
^o Q ₁ (7)	5947.4269	0.0055	^r Q(1)	5950.7738	0.0277
^o Q ₁ (6)	5947.4338	0.0081	^r Q(1)	5950.7793	0.0202
^o Q ₁ (1)	5947.4381	0.0321	^o R ₁ (5)	5950.9890	0.2467
^o Q ₁ (5)	5947.4397	0.0159	^o R ₂ (5)	5950.9929	0.0147
^o Q ₁ (4)	5947.4440	0.0393	^o R ₂ (5)	5950.9942	0.0151
^o Q ₁ (2)	5947.34449	0.0511	^o R ₂ (5)	5950.9964	0.0175
^o Q ₂ (3)	5947.4459	0.0375	^o R ₀ (2)	5951.0031	0.2219

upper state appeared fractionated, the centers of gravity of all assigned lines sharing the same quantum numbers were used in the fit.

In Table 4 we list the coupling matrix elements for the perturbing states, along with the centers of gravity for each J . The matrix elements were determined using a modified [31] Lawrance–Knight deconvolution

method [32]. The errors in the table were calculated propagating a frequency error of 9 MHz, a relative intensity fluctuation of 10% and a baseline uncertainty of 2% for the strongest peaks. Note that for the $K=1$, $J'=4$ pair, only one coupling matrix element is given for the P branch compared to two for the R branch. This is due to the fact that the third transition in the P

Table 3
Results of the fit of the individual bands in the 5947.5 cm⁻¹ region

Sub-band	Sub-band origin (cm ⁻¹)	ΔB (cm ⁻¹)	σ ($\times 10^4$ cm ⁻¹)
$K=0$	5947.4704(1)	-0.00057(1.5)	2.0
$K=1$	5947.4560(3)	-0.00053(0.1)	3.7
$K=2$	5947.4712(18)	-0.00079(0.7)	24.2

Groundstate constants from Ref. [25] were used: $B_0=0.29627693$ cm⁻¹; $D_j=0.88401 \times 10^{-7}$ cm⁻¹; $D_{JK}=0.54490 \times 10^{-5}$ cm⁻¹.

branch pair coincides exactly with the much stronger P₀(5) line. The comparison of the matrix elements for the two branches gives an indication of the precision of the relative intensities since these are entered into the deconvolution procedure. As it can be seen, the matrix elements for the P and R branches generally agree to within 15%. In a recent publication [5], McIlroy et al. derived an expression for the experimental density of states that corrects for bias created by a finite signal to noise ratio in the observed spectrum. It has the following form:

$$\rho_{\text{coupled}} = \frac{\sum_i (V_i)^{-1}}{2N_B \sqrt{S/N}} \quad (2)$$

Table 4
Comparison of the coupling matrix elements for R branch and P branch transitions in the 5947.5 cm⁻¹ band

J'	K	R branch (cm ⁻¹)	Matrix element ($\times 10^4$ cm ⁻¹)	P branch (cm ⁻¹)	Matrix element ($\times 10^4$ cm ⁻¹)
0	0			5946.8784 \pm 0.0013	39 \pm 30
1	0	5948.0823 \pm 0.0032	163 \pm 148		
1	1			5946.2701 \pm 0.0014	34 \pm 22
					38 \pm 18
2	1	5948.6377 \pm 0.0003	24 \pm 2	5945.6747 \pm 0.0004	24 \pm 4
3	1	5949.2279 \pm 0.0011	30 \pm 16	5945.0796 \pm 0.0031	43 \pm 8
			12 \pm 5		11 \pm 16
			35 \pm 45		41 \pm 113
4	1	5949.8159 \pm 0.0008	42 \pm 9	5944.4828 \pm 0.0014	41 \pm 19
			19 \pm 8		
2	2			5945.6912 \pm 0.0154	193 \pm 30
					7 \pm 7
3	2	5949.2364 \pm 0.0092	186 \pm 92	5945.0919 \pm 0.0118	194 \pm 23
4	2	5949.8282 \pm 0.0082	189 \pm 39	5944.4935 \pm 0.0136	176 \pm 89
5	2	5950.4071 \pm 0.0031	35 \pm 35	5943.8900 \pm 0.0053	32 \pm 68
			6 \pm 2		5 \pm 3
6	2	5950.9946 \pm 0.0011	8 \pm 3	5943.2921 \pm 2921	8 \pm 5
			12 \pm 3		12 \pm 7

The numbers in the same row as the K and J' quantum numbers are the centers of gravity. Listed beside these are the coupling matrix elements in units of 10^{-4} cm⁻¹. The uncertainties were found by propagation of a 9 MHz frequency error, a 2% baseline intensity error and a 10% relative intensity error. All the data are taken from the same sub band (D) except the $K=2$, $J'=3$ data are from another sub-band (E).

where V_i are the individual coupling matrix elements, as determined by the Lawrance–Knight deconvolution and N_B is the number of bright states. With a signal to noise ratio of about 60 across our entire spectrum, we calculate an experimental density of states of 57.8 ± 5.4 (3σ) states per cm⁻¹. We calculated a total of 27 vibrational states per cm⁻¹, using a regularized inverse Laplace transform [33] applied to the fundamental frequencies in Table 1. This includes states of all possible symmetries. If one assumes the coupling to be anharmonic, only states of B₂ symmetry should be considered. The density of states with this symmetry is then only $27/6=4.5$ states per cm⁻¹ [34]. However, we do not have an estimate for the anharmonicities in allene, and therefore did not include these in our calculation. At these energies, for propyne there is a 30% increase in the density of states when one includes (diagonal) anharmonicities in the calculation. Assuming a similar increase in allene, the calculated density of B₂ vibrational states would go up to about 6 states per cm⁻¹, which obviously is not enough to make up for the discrepancy. Parallel Coriolis interactions, which are expected for $K>0$ upper states, will mix the B₁ and B₂ symmetry vibrational states, thus increasing

the expected density of states to ~ 12 states per cm^{-1} . The $2\nu_1$ spectrum of propyne displays strong Coriolis interactions [5]. Perpendicular Coriolis interactions could lead to a breakdown of all selection rules based on vibrational symmetry, leading to a predicted density that will grow linearly with J . Such interactions are often invoked to explain an observed density of states much larger than an estimated density of vibrational states. Given the large fluctuations observed in the coupling matrix elements in the present spectrum (and the fact that the experimental density is affected most strongly by the weakest interaction matrix element since such states must be quite close to a bright state to produce observable transitions), we cannot rule out such an explanation. However, there appears to be no systematic increase with J in the degree of fractionation of the lines in the allene $\nu_1 + \nu_5$ band.

Another possible explanation for an experimental density of states to exceed the estimated one is statistical fluctuations. Such fluctuations may be expected to be large especially in symmetric tops, due to the high degeneracy of levels in the harmonic limit. From an explicit harmonic calculation of all levels in the region near 5950 cm^{-1} , we find that on average, each level has a degeneracy of about 7, due to the many possible values for the vibrational angular momenta in each of the E symmetry modes. Anharmonic terms in the potential will lift the degeneracy of such levels, due to the g_{ij} and vibrational l -resonance terms. These are typically an order of magnitude smaller than the x_{ij} anharmonic terms. These clusters of bath states will be strongly coupled among themselves by Coriolis interactions. Fig. 3 shows a plot of a convolution of the calculated ‘stick’ spectrum of harmonic states with a 5 cm^{-1} FWHM Gaussian function. The width of the Gaussian was rather arbitrarily chosen to model the splitting of the l -degeneracy of each bath state. It is seen that fluctuation of a factor of two in the bath state density occur, even though on average there are about 100 states under the Gaussian width, and thus one would have expected fluctuations in the density of only $\sim 20\%$ if the level positions were uncorrelated. First order Coriolis interactions among bath states could result in a predicted effective density of states in the spectrum on the order of 20–40 states per cm^{-1} , within the range of value deduced from the spectrum. This proposed type of first order Coriolis mixing is distinct from the strong Coriolis mixing that lead to a complete breakdown of K as

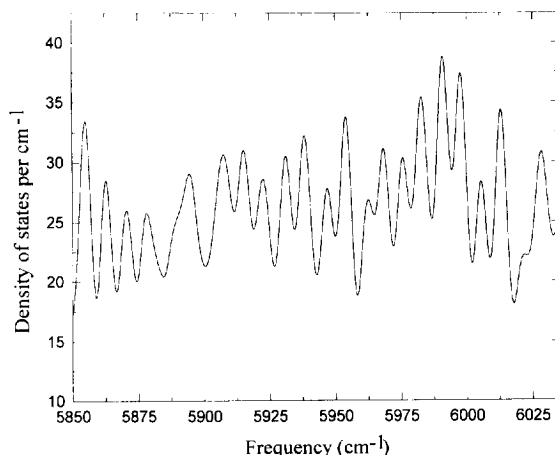


Fig. 3. Density of states per cm^{-1} as function of the frequency for the region around 5945 cm^{-1} . The densities were calculated by direct count and convoluted with a 5 cm^{-1} FWHM Gaussian.

a useful quantum number, and a linear increase of the density of states. Here, each ro-vibrational state has a population primarily in one K value, but can mix states differing by $K=0, \pm 1$. Such mixing among the bath levels will be very difficult to detect directly in a sparse spectrum, since the effective density of bath states will saturate at very low J and K . This appears to be the best explanation of the observed density, but in such sparse spectra it is important to recognize the limited information provided by the spectrum, which makes all such conclusions tentative.

It is conceptually useful to connect the spectroscopic perturbations with a dynamical picture of the time evolution of the excitation of an initial state, $\nu_1 + \nu_5$ in the present case. When only a few perturbing states are present, the time evolution of a coherent excitation shows quantum beats between the levels involved without a relaxation: i.e. the energy is sloshing in and out of those states. Thus one can not give a lifetime for the survival of the energy in the initially excited state. However, if one considers the rms average of the observed perturbation(s), it is possible to obtain an effective lifetime by using Fermi's Golden Rule:

$$\tau_{\text{GR}} = (4\pi^2 c \rho V_{\text{rms}}^2)^{-1}. \quad (3)$$

With $\langle V_{\text{rms}} \rangle = 8.19 \times 10^{-3} \text{ cm}^{-1}$ and $\rho = 57$ states per cm^{-1} , we find $\tau_{\text{GR}} \approx 220 \text{ ps}$ which is similar to the lifetime typically observed for an acetylenic C–H excitation. For example, the first overtone band of

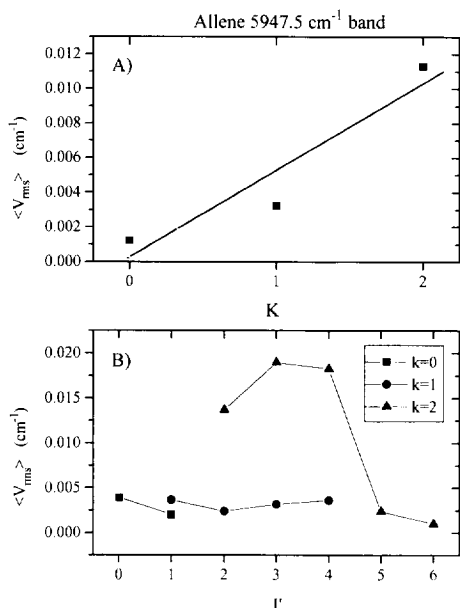


Fig. 4. Dependence of the root mean square matrix element upon (a) K , averaged over all J' , and (b) J' , for individual K . The line drawn in (a) is a linear fit of the three data points.

$(\text{CH}_3)_2\text{C}=\text{C}\equiv\text{CH}$ has a lifetime of 110 ps [36], and the second overtone of propyne has a lifetime of 300 ps for $K=0$ levels [5].

In order to establish whether Coriolis coupling is present in this band, we plotted the size of the coupling matrix elements $\langle V_{rms} \rangle$ as a function of both K and J' (Figs. 4a, 4b). In the case of first order parallel (z -axis) Coriolis coupling, the size of the matrix coupling elements is zero for $K=0$ and increases linearly with K for $K \neq 0$. As it can be seen from Fig. 4a, the increase of the rms matrix elements as a function of K is consistent with a linear dependence. However, as Fig. 4b shows, the $\langle V_{rms} \rangle$ for $K=2$, $J'=5, 6$ are similar to those of $K=0$ and 1. The large values for $K=2$, $J'=2-4$ may reflect the contribution of a particularly strongly coupled bath state that detunes with increasing J' . This bath state is not identified for $J' > 4$ since it will be outside the region of the assigned clump. Thus given the sparse data and large fluctuations, we can not definitively say if there is a systematic K dependence to $\langle V_{rms} \rangle$. It is interesting to note that the $2\nu_1$ band of propyne also displays an apparent parallel Coriolis interaction with nearby degenerate bath states. This was attributed to the presence of at least one doorway state which could be present in allene as well.

Fig. 4b shows the dependence of the size of the coupling matrix elements as a function of J . Perpendicular Coriolis interactions (x, y) between B_2 vibrational states would result in an increase of the matrix elements with $\sqrt{J(J+1) - K(K+1)}$ [7]. Since we do not observe such a dependence, we can conclude that x, y Coriolis interactions do not play an important role in coupling the $\nu_1 + \nu_5$ state to the bath of iso-energetic states. The effect of Coriolis interactions between the bath states produces a decrease in the size of the effective coupling matrix elements with J , but this could be difficult to detect for weak Coriolis mixing.

3.2. The $2\nu_8$ region

Fig. 5 shows the spectrum of allene in the $2\nu_8$ region around 6135.5 cm^{-1} . It is obvious that the spectrum is much more complicated here than in the $\nu_1 + \nu_5$ region. Closer examination of the spectrum reveals that at least six sub bands, marked A through F, can be resolved. Fig. 6 shows a blow up of the spectrum including the individual sub bands A through E. We were able to assign more than 95% of the strong lines and about 50% of all transitions observed. Again, assignments were made using the method of ground state combination differences with the ground state constants from Ref. [25]. Table 5 contains the complete list of the frequency and relative intensity of all assigned lines. Accuracy of the absolute frequency is $\pm 0.005 \text{ cm}^{-1}$, while the relative intensities are accurate to about 10%.

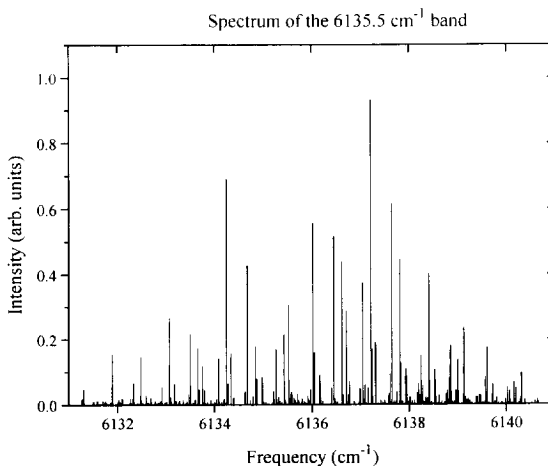


Fig. 5. Spectrum of the $2\nu_8$ band in allene. The spectrum is more complicated in this region than for the lower energy $\nu_1 + \nu_5$ band.

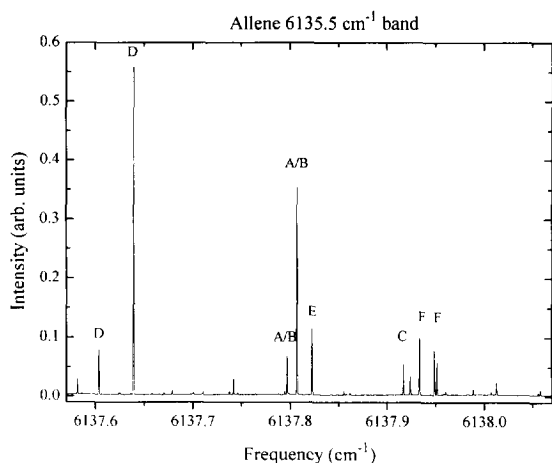


Fig. 6. Blow-up of the $2\nu_8$ spectrum, showing the individual sub-bands, marked A–F. The Hönl–London factors are too small to distinguish the A and B sub-bands at this J' .

Only one of the six bands (D) is considerably perturbed, while three other bands (B, E and F) are only very weakly perturbed. For $J' > 4$ we were not able to make rigorous assignments for the $K=0$ and $K=1$ components of the A and B band since the Q branch Hönl–London factors are too small for the $K=1$ states to be distinguished from $K=0$ by the Q line in the former. All six bands were individually fit to the symmetric top energy levels from Eq. (2). Again, we were not able to fit the ΔD_J value without increasing the value of σ^2 , and therefore did not include this variable in the final fits. The results are presented in Table 6.

The coupling matrix elements were determined using the modified Lawrance–Knight deconvolution for each of the individual perturbed bands. They are listed in Table 7. Again, the errors in the table were calculated propagating a frequency error, a relative intensity, and an absolute intensity variation of 9 MHz, 10% and 2% respectively.

As it can be seen in Fig. 7a, there is no systematic dependence of the rms matrix element as of function of K . Thus we conclude that unlike for the 5947.5 cm^{-1} band, z -axis Coriolis coupling does not play an important role in this region. From Fig. 7b we can also see that the size of the rms matrix element also does not scale with J as $\sqrt{J(J+1) - K(K+1)}$, indicating that there is minimal perpendicular type Coriolis coupling.

Using Eq. (1), with $N_B = 16$, and average signal to noise of 50, and a rms coupling matrix elements size

of $1.52 \times 10^{-4}\text{ cm}^2$, we find an experimental density of states of 31.0 ± 4.3 (3σ) states per cm^{-1} . The calculated harmonic density of vibrational states is 32 states per cm^{-1} , and correction for diagonal anharmonicity (as above for the lower energy band) should increase this 30% to 42 states per cm^{-1} , of which 7 should be of B_2 symmetry.

A calculation of the average degeneracy and level clustering in this band produces results similar to those discussed above for the other band. As before, the most natural explanation for the observed density being close to the calculated total density of vibrational states (of all symmetries), is to assume weak first order Coriolis interactions among the bath states so that the B_2 symmetry vibrational level can couple to vibrational levels of B_2 , B and E symmetry. The total density of such vibrational states is about ~ 20 states per cm^{-1} , which is consistent with the observed value, considering the expected fluctuations. It is interesting that the observed density of states is about half as large for this band compared to the lower energy $\nu_1 + \nu_5$ band, despite the fact that the higher energy band is more perturbed. This is an indication of the importance of fluctuations in the observed density of states. For spectra with the statistical properties of the Gaussian orthogonal ensemble (expected for chaotic classical dynamics), fluctuations in level density are greatly reduced [35,36]. Thus the observed fluctuations in both level density and observed matrix elements suggest that the classical dynamics of allene is regular in this energy region.

Considering now the splitting of the $K=0$ transition strength into three sub-bands, we can estimate the rate of energy transfer out of the initially bright state. Since we observe three $K=0$ bands (three eigenstates), we suspect the existence of two perturbing states in the first tier. As mentioned before, in the limit of only a few perturbing states, the time evolution of a coherent excitation is a quantum beat between the levels involved. This quantum beat averaged over J is shown in Fig. 8. The figure shows that the initially excited state becomes almost completely depopulated after about 40 ps, but shows strong recurrences thereafter. The rms coupling matrix element between the states in this case is 0.402 cm^{-1} . Interestingly, we find that if we consider only the first tier states, we get an experimental density of states which is very close to the calculated B_2 vibrational density: 6 and 7 states per cm^{-1} respectively (including a correction for the anharmonicity). By

Table 5

Frequency and relative intensity of the assigned lines in the 6135.5 cm⁻¹ region. The last column indicates the sub-band to which the line belongs

	Frequency (cm ⁻¹)	Relative intensity	Band		Frequency (cm ⁻¹)	Relative intensity	Band
^o P(7)	6131.2643	0.0160	A/B	^o R ₀ (0)	6135.9705	0.0449	B
^o P(7)	6131.2935	0.0351	A/B	^o R ₀ (0)	6136.0238	0.5552	B
^o P(7)	6131.3035	0.0466	A/B	Q ₂ (4)	6136.0484	0.0045	E
^o P ₀ (7)	6131.6966	0.0110	D	Q ₂ (4)	6136.0504	0.0143	E
^o P ₀ (7)	6131.6999	0.0090	D	Q ₂ (3)	6136.0525	0.0394	E
^o P ₀ (7)	6131.7439	0.0076	D	Q ₂ (2)	6136.0539	0.1589	E
^o P ₀ (7)	6131.7574	0.0103	D	^o P ₀ (2)	6136.1612	0.0896	F
^o P(6)	6131.8839	0.0655	A/B	^o P ₀ (2)	6136.1792	0.0502	F
^o P(6)	6131.8917	0.1533	A/B	^o R ₀ (0)	6136.4035	0.0500	D
^o P ₀ (6)	6132.2708	0.0172	D	^o R ₀ (0)	6136.4507	0.5158	D
^o P ₀ (6)	6132.3122	0.0181	D	^o R ₁ (1)	6136.6171	0.3046	A
^o P ₀ (6)	6132.3322	0.0661	D	^o R ₀ (1)	6136.6191	0.4378	B
^o P ₀ (6)	6132.3413	0.0041	D	^o R ₁ (1)	6136.7087	0.2876	C
^o P(5)	6132.4691	0.0279	A/B	^o P ₀ (1)	6136.7733	0.0714	F
^o P(5)	6132.4794	0.1460	A/B	^o R ₀ (1)	6137.0044	0.0462	D
^o P ₂ (6)	6132.4888	0.0097	E	^o R ₀ (1)	6137.0466	0.3739	D
^o P ₁ (5)	6132.5890	0.0291	C	^o R ₁ (2)	6137.2144	0.2490	A
^o P ₀ (8)	6132.6037	0.0044	F	^o R ₀ (2)	6137.2154	0.9309	B
^o P ₀ (5)	6132.8851	0.0106	D	^o R ₁ (2)	6137.3119	0.1895	C
^o P ₀ (5)	6132.9097	0.0076	D	^o R ₀ (2)	6137.6090	0.0934	D
^o P ₀ (5)	6132.9128	0.0537	D	^o R ₀ (2)	6137.6304	0.0049	D
^o P ₁ (4)	6133.0669	0.1201	A	^o R(3)	6137.8024	0.0726	A/B
^o P ₀ (4)	6133.0678	0.2690	B	^o R(3)	6137.8126	0.4457	A/B
^o P ₂ (5)	6133.0839	0.0117	E	^o R ₂ (2)	6137.8280	0.1255	E
^o P ₂ (5)	6133.0859	0.0217	E	^o R ₁ (3)	6137.9220	0.0863	C
^o P ₁ (4)	6133.1643	0.0631	C	^o R ₀ (0)	6137.9388	0.1086	F
^o P ₀ (7)	6133.1901	0.0114	F	^o R ₀ (0)	6137.9567	0.0658	F
^o P ₀ (7)	6133.2025	0.0102	F	^o R ₀ (3)	6138.2177	0.0294	D
^o P ₀ (4)	6133.4613	0.0316	D	^o R ₀ (3)	6138.2420	0.0204	D
^o P ₀ (4)	6133.4969	0.2163	D	^o R ₀ (3)	6138.2455	0.1489	D
^o P ₁ (3)	6133.6543	0.1259	A	^o R(4)	6138.4020	0.1810	A/B
^o P ₀ (3)	6133.6564	0.1706	B	^o R(4)	6138.4097	0.4004	A/B
^o P ₂ (4)	6133.6804	0.0456	E	^o R ₂ (3)	6138.4164	0.0207	E
^o P ₁ (3)	6133.7462	0.1186	C	^o R ₂ (3)	6138.4185	0.0704	E
^o P ₀ (6)	6133.7921	0.0442	F	^o R ₁ (1)	6138.5326	0.1055	F
^o P ₀ (3)	6134.0416	0.0157	D	^o R ₀ (4)	6138.7890	0.0436	D
^o P ₀ (3)	6134.0838	0.1404	D	^o R(5)	6138.7995	0.0154	A/B
^o P ₀ (2)	6134.1926	0.0187	B	^o R ₀ (4)	6138.8304	0.0806	D
^o P ₁ (2)	6134.2425	0.1205	A	^o R ₀ (4)	6138.8502	0.1799	D
^o P ₀ (2)	6134.2460	0.6905	B	^o R ₀ (4)	6138.8589	0.0066	D
^o P ₂ (3)	6134.2750	0.0649	E	^o R(5)	6138.9669	0.0427	A/B
^o P ₁ (2)	6134.3332	0.1574	C	^o R(5)	6138.9962	0.0904	A/B
^o P ₀ (5)	6134.3850	0.0199	F	^o R ₂ (4)/ ^o R(5)	6139.0063	0.1367	E A/B
^o P ₀ (2)	6134.6256	0.0394	D	^o R ₀ (2)	6139.1250	0.0447	F
^o P ₀ (2)	6134.6729	0.4270	D	^o R ₀ (5)	6139.4027	0.0211	D
^o P ₀ (1)	6134.8370	0.1791	B	^o R ₀ (5)	6139.4469	0.0283	D
^o P ₀ (4)	6134.9779	0.0827	F	^o R ₀ (5)	6139.4604	0.0295	D
^o P ₀ (1)	6135.2638	0.1680	D	^o R ₀ (5)	6139.4711	0.0268	D
Q ₁ (1)	6135.4275	0.2151	A	^o R(6)	6139.5671	0.0823	A/B
Q ₁ (2)	6135.4320	0.0858	A	^o R(6)	6139.5965	0.0371	A/B
Q ₁ (3)	6135.4369	0.0347	A	^o R(6)	6139.6015	0.1735	A/B
Q ₁ (1)	6135.5183	0.3070	C	^o R ₀ (3)	6139.7178	0.0610	F
Q ₁ (2)	6135.5237	0.0747	C	^o R ₀ (6)	6140.0182	0.0509	D
Q ₁ (3)	6135.5341	0.0198	C	^o R ₀ (6)	6140.0672	0.0405	D
Q ₁ (4)	6135.5521	0.0052	C	^o R ₀ (4)	6140.3100	0.0967	F
^o P ₀ (3)	6135.5699	0.0382	F				

Table 6

Results of the fits of the individual sub bands observed in the 6135.5 cm^{-1} region. Including ΔD_j resulted in an unacceptable large values for σ^2

Sub-band	K	Sub-band origin (cm^{-1})	ΔB (cm^{-1})	σ ($\times 10^{-4} \text{ cm}^{-1}$)
A	1	6135.4252(2)	0.0012(1)	1.18
B	0	6135.42819(8)	0.0008(2)	16.0
C	1	6135.5158(2)	0.0012(0.4)	1.36
D	0	6135.8509(39)	0.0007(1)	95.2
E	2	6136.0549(2)	-0.0004(1)	2.73
F	0	6137.3531(18)	-0.002(0.8)	45.4

using Fermi's Golden Rule, we also calculated the effective lifetime as we did for the 5947.5 cm^{-1} band, considering coupling out of each of the three $K=0$ states independently, i.e. the 0.16 cm^{-1} coupling matrix elements are not included. With a rms coupling matrix element of $1.234 \times 10^{-3} \text{ cm}^{-1}$ and an experimental density of states of 32 per cm^{-1} , we find $\tau_{\text{GR}} \approx 180 \text{ ps}$, slightly shorter than the 220 ps for the lower energy band. However, given the limited statistics for both bands, these two lifetimes should be viewed as essentially equal.

In order to get an estimate of the number of states that were available for low order resonances, we calculated all possible states in a 100 cm^{-1} window

around 6135.5 cm^{-1} . Anharmonicities and Darling–Dennison terms were not included. Then we determined the symmetry of all states, and selected those with B_2 symmetry, i.e. those states that can couple to the bright state. Lastly, we determined the order of coupling to the bright state of each state with B_2 symmetry. Table 8 lists the results and compares them to the acetylenic C–H stretch overtones of several other molecules. As can be seen from the table, in allene the number density of low order resonances is very small. Compared to propyne, allene has a similar density of states and number of low order resonances, and the lifetimes are on the same order of magnitude. The perturbations in the low energy $\nu_1 + \nu_5$ and high energy

Table 7

Same as Table 2 except now for the $2\nu_8$ region

Band	J'	K	R branch (cm^{-1})	Matrix element ($\times 10^4 \text{ cm}^{-1}$)	P branch (cm^{-1})	Matrix element ($\times 10^4 \text{ cm}^{-1}$)
D	1	0	6136.4465 ± 0.0016	134 ± 24	6134.6689 ± 0.0020	131 ± 29
	2	0	6137.0420 ± 0.0019	132 ± 24	6134.0795 ± 0.0049	127 ± 65
	3	0	6137.6101 ± 0.0042	47 ± 86	6133.4924 ± 0.0026	119 ± 29
	4	0	6138.2410 ± 0.0024	97 ± 25	6132.9084 ± 0.0066	97 ± 67
				13 ± 5		11 ± 11
	5	0	6138.8367 ± 0.0037	184 ± 32	6132.3191 ± 0.0105	205 ± 85
				101 ± 7		94 ± 30
			18 ± 26		24 ± 52	
	6	0	6139.4480 ± 0.0100	216 ± 66	6131.7234 ± 0.0282	253 ± 60
				86 ± 15		98 ± 55
				68 ± 13		23 ± 12
	7	0	6140.0399 ± 0.0078	244 ± 9		
B	1	0	6136.0198 ± 0.0017	140 ± 28	6134.2446 ± 0.0015	86 ± 44
E	4	2	6138.4181 ± 0.0004	9 ± 3	6133.0852	10 ± 3
F	2	0	6137.9456 ± 0.0016	87 ± 5	6136.1677	87 ± 6
	6	0			6133.1960 ± 0.0081	62 ± 5

All matrix elements are from the same band, except for the last two, which are from band A/B and band E respectively. The uncertainties were found by propagation of a 9 MHz frequency error, a 2% baseline intensity error and a 10% relative intensity error.

Table 8
IVR lifetimes and calculated density of states for the C–H stretch overtones of allene and the acetylenic C–H stretch of several acetylenic compounds

Molecule	Lifetime (ps)	Density of states ($1/\text{cm}^{-1}$) ^a	Low order resonances number density ($1/\text{cm}^{-1}$)		
			3rd order	4th order	5th order
$\text{H}_2\text{C}=\text{C}=\text{CH}_2$	185	42	0.00	0.03	0.77
$\text{CH}_3-\text{C}\equiv\text{CH}$	5000	66	0.00	0.00	0.05
$(\text{CH}_3)_3\text{Si}-\text{C}\equiv\text{CH}$ ^c	2000	2.0×10^4	0.15	2.66	19.23
$(\text{CH}_3)_3\text{Sn}-\text{C}\equiv\text{CH}$ ^c	6000	6.0×10^5	0.03	2.71	19.32
$(\text{CH}_3)_3\text{C}-\text{C}\equiv\text{CH}$ ^d	110 ^b	6.2×10^5	0.24	2.32	18.05
$(\text{CD}_3)_3\text{C}-\text{C}\equiv\text{CH}$ ^d	<20 ^b	7.6×10^6	0.30	3.32	31.89
$(\text{CF}_3)_3\text{C}-\text{C}\equiv\text{CH}$ ^d	5(?) ^b	1.0×10^{11}	0.03	1.38	42.24

^a Calculated total density of states. ^b Determined from experimental decay curves, others by Fermi's Golden Rule.

^c From Ref. [37]. ^d From Ref. [38].

$2\nu_8$ bands in allene are comparable to those in the weakly perturbed $2\nu_1$ band and the more extensively perturbed $2\nu_6$ band respectively in propyne.

4. Conclusions

The $\nu_1 + \nu_5$ band in allene shows a very small perturbation for $R_0(0)$ and $P_0(1)$, which disappears upon

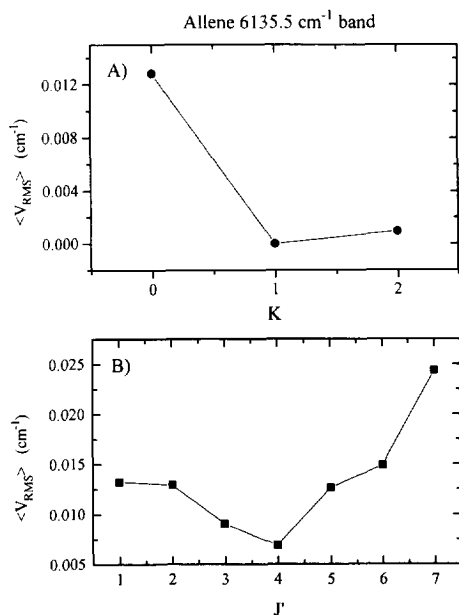


Fig. 7. Shown here is $\langle V_{rms} \rangle$ versus K (a) and J' (b). Neither plot shows a linear dependence upon K or J' ($J' + 1$), indicating minimal parallel and perpendicular Coriolis coupling.

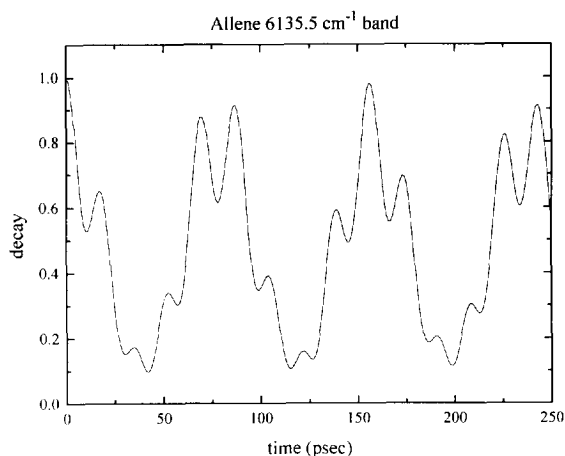


Fig. 8. Quantum beats as calculated for the fast energy transfer out of the $2\nu_8$ excited state. The $1/e$ time is approximately 25 ps.

increase of J' . In analogy to propyne, which displayed a similar behavior in the $2\nu_1$ band, we suspect the presence of a doorway state which causes interaction with nearby degenerate bath states. Based on the lack of a systematic increase of the coupling matrix elements with J' , we suspect that perpendicular Coriolis interactions do not play an important role in the $\nu_1 + \nu_5$ band.

The spectrum in the $2\nu_8$ region is more complicated than in the lower energy $\nu_1 + \nu_5$ band. We were able to identify six sub-bands: three $K=0$, two $K=1$, and one $K=2$ band(s). Only one of these bands was considerably perturbed. Unlike in the case of the 5947.5 cm^{-1} band, there are no parallel Coriolis interactions

apparent. Since there is no obvious dependence of the coupling matrix elements upon J' and K , we suspect that neither parallel nor perpendicular Coriolis interactions are important in this band. Because we observe three $K=0$ bands, we expect the existence of two perturbing states in the first tier. The initial bright state becomes almost completely depopulated at a timescale of about 40 ps but the bright state population shows strong recurrences thereafter.

The effective lifetime for the C–H stretch overtones, calculated using Fermi's Golden Rule, is about 200 ps for both bands. Based on the very small number density of low order resonances for the $2\nu_8$ band, one might expect a longer lifetime. However, the lifetime of the overtone of the C–H stretch in allene is near the middle of the range of lifetimes that have been observed for the acetylenic stretch overtone in molecules studied previously in our laboratory.

Acknowledgements

The authors would like to thank Joan Gambogi for assisting with the recording of the spectra, Dr. Ian Mills for the permission to reproduce his spectrum, and Dr. Michel Herman for supplying high resolution FTIR spectra. This work was funded by the NSF.

References

- [1] K.K. Lehmann, B.H. Pate and G. Scoles, Intramolecular dynamics from eigenstate-resolved infrared spectra, *Ann. Rev. Phys. Chem.* 45 (1994) 241.
- [2] A.M. de Souza, D. Kaur and D.S. Perry, *J. Chem. Phys.* 88 (1987) 4569.
- [3] A. McIlroy and D.J. Nesbitt, *J. Chem. Phys.* 91 (1989) 104.
- [4] E.R.Th. Kerstel, K.K. Lehmann, B.H. Pate and G. Scoles, *J. Chem. Phys.* 100 (1994) 2588.
- [5] A. McIlroy, D.J. Nesbitt, E.R.Th. Kerstel, K.K. Lehmann and G. Scoles, *J. Chem. Phys.* 100 (1994) 2596.
- [6] J. Go, T.J. Cronin and D.S. Perry, *Chem. Phys.* 175 (1993) 127.
- [7] J.E. Gambogi, E.R.Th. Kerstel, K.K. Lehmann and G. Scoles, *J. Chem. Phys.* 100 (1994) 2612.
- [8] G.A. Bethardy, X. Wang and D.S. Perry, *Can. J. Chem.* 72 (1994) 652.
- [9] J.J. Gajewski, *Hydrocarbon thermal isomerization* (Academic Press, New York, 1981) p. 21.
- [10] J. Overend and H.W. Thompson, *J. Opt. Soc. Am.* 43 (1953) 1065.
- [11] J. Overend and H.W. Thompson, *Trans. Faraday Soc.* 52 (1956) 1295.
- [12] J. Overend and B. Crawford, *J. Chem. Phys.* 29 (1958) 1002.
- [13] S. Brodersen and E.H. Richardson, *J. Mol. Spectry.* 4 (1960) 439.
- [14] I.M. Mills and J.L. Duncan, *J. Mol. Spectry.* 9 (1962) 244.
- [15] I.M. Mills, W.L. Smith and J.L. Duncan, *J. Mol. Spectry.* 16 (1965) 349.
- [16] A.G. Maki and R.A. Toth, *J. Mol. Spectry.* 17 (1965) 136.
- [17] G.J. Cartwright and I.M. Mills, *J. Mol. Spectry.* 34 (1970) 415.
- [18] R.J. Butcher and W.J. Jones, *J. Raman Spectry.* 1 (1973) 393.
- [19] F. Hegelund, J. Bendtsen and N.R. Zangenberg, *J. Raman Spectry.* 2 (1974) 31.
- [20] F. Hegelund, J.L. Duncan and D.C. McKean, *J. Mol. Spectry.* 65 (1977) 366.
- [21] J. Pliva and J. Kauppinen, *J. Mol. Spectry.* 111 (1985) 93.
- [22] A.G. Maki, A.S. Pine and M. Dang-Nhu, *J. Mol. Spectry.* 112 (1985) 459.
- [23] W. Knippers, K. van Helvoort, M. de Felici, J. Reuss and S. Stolte, *Chem. Phys.* 105 (1986) 27.
- [24] F. Hegelund, R. Anttila and S. Alanko, *J. Mol. Spectry.* 141 (1990) 309.
- [25] F. Hegelund, N. Andresen and M. Koivusaari, *J. Mol. Spectry.* 149 (1991) 305.
- [26] T.E. Gough, R.E. Miller and G. Scoles, *Appl. Phys. Letters* 30 (1977) 338.
- [27] M. Zen, in: *Atomic and molecular beam methods*, Vol. 1, ed. G. Scoles (Oxford Univ. Press, New York, 1988).
- [28] E.R.Th. Kerstel, K.K. Lehmann, B.H. Pate and G. Scoles, *J. Phys. Chem.* 95 (1991) 8282.
- [29] Nguyen van Than, *Ann. Phys.* 2 (1969) 241.
- [30] I.M. Mills and F.J. Mompean, *Chem. Phys. Letters* 124 (1986) 425.
- [31] K.K. Lehmann, *J. Chem. Phys.* 95 (1991) 7556.
- [32] W.D. Lawrance and A.E. Knight, *J. Chem. Phys.* 89 (1985) 917.
- [33] D. Romanini and K.K. Lehmann, *J. Chem. Phys.* 98 (1993) 6437.
- [34] M. Quack, *J. Chem. Phys.* 82 (1985) 3277.
- [35] J.E. Gambogi, R.P. L'Esperance, K.K. Lehmann, B.H. Pate and G. Scoles, *J. Chem. Phys.* 98 (1993) 1112.
- [36] K.K. Lehmann and S.L. Coy, *Ber. Bunsenges. Physik. Chem.* 92 (1988) 306.
- [37] B.H. Pate, PhD Thesis, Princeton University (1992).
- [38] J.E. Gambogi, K.K. Lehmann, B.H. Pate, G. Scoles and X. Yang, *J. Chem. Phys.* 98 (1993) 1748.